Metal Penetration in Sand Molds: A Fundamental Approach to Solving the Problem

AFS Research

D.M. Stefanescu
T.S. Piwonka
S. Giese
A. Lane
University of Alabama
Tuscaloosa, Alabama

ABSTRACT

A mathematical model that describes metal penetration in sand molds is introduced. The model is based on a pressure balance. It demonstrates that the main force opposing penetration is the capillary force, and that the main parameter is the contact angle between the liquid metal and the mold material. It is also shown that the capillary force can be dramatically influenced by temperature, metal composition, composition of atmosphere at the mold/metal interface and casting size.

The model explains and quantifies the role of foundry variables, such as mold hardness, AFS grain size, type of sand, sand additives, metallostatic pressure, physical properties of the metal and pouring height. Various types of penetration, such as mechanical or chemical, are explained on the basis of the model. Experimental methods for evaluation of the data required for prediction of occurrence of metal penetration are outlined. Typical examples of such data are given.

INTRODUCTION

Metal penetration into sand molds is a defect that has been present in sand castings since the beginning of metalcasting. The defect can vary in severity from a rough casting surface to a tightly bonded mixture of sand and metal that firmly adheres to the casting. The defect is estimated to cost American foundries 60 million annually.

Previous studies of metal penetration[1-6] identified two major mechanisms of penetration: mechanical penetration (which results when the metallostatic head forces metal into the pores between sand grains) and chemical penetration (which occurs when metal reacts with the sand, often with the help of the atmosphere). Oxidizing atmospheres have been shown to promote penetration, while reducing atmospheres retard it. This is one of the reasons that seacoal is added to sand mixes.

However, it has been clear for many years that merely providing a reducing atmosphere is not sufficient to prevent penetration defects. In addition, the defect has been shown to be sensitive to metal composition. The conclusion is that penetration is a complex phenomena that has no simple answer. The work reported in this paper is the result of a study that has attempted to describe penetration in terms of the physics and chemical reactions that take place at the mold-metal interface—including the effects of mold atmosphere, metal chemistry, mold chemistry and heat transfer—in an effort to understand the defect so that it can be prevented.

PENETRATION MODEL

The penetration model that will be introduced in this paper is a further development of the model proposed earlier.[7] A graphic description of the problem to solve is provided in Fig. 1. The liquid metal may be pushed into the molding aggregate by a combination of static (P_{st}) and dynamic (P_{dyn}) pressures. The pressures opposing penetration are the pressure drop resulting from the friction between the liquid metal and the sand grains (P_f) and the pressure resulting from the expansion of the gases in the mold (P_{gas}). If the metal wets the sand grains, a capillary pressure (P_γ) may also contribute to penetration. When the metal does not wet the molding aggregate, the capillary pressure will oppose penetration. The governing equation that describes the penetration of liquid metal into a molding aggregate is thus:

$$P_{st} + P_{dyn} + P_\gamma = P_f + P_{gas} \quad (1)$$

When the left-hand side of Equation 1 is larger than the right-hand side, penetration will occur. Each of the terms of Equation 1 must now be calculated. Neglecting the gas pressure for the time being, the appropriate equations are as follows:

$$P_{st} = \rho_L g h \quad (2)$$

$$P_{dyn} = R_p \rho_L [2g(H - h)]^{0.5} \quad (3)$$

$$P_\gamma = \frac{4}{d_e} \gamma_{LV} \cos\theta \quad (4)$$

$$P_f = \frac{\mu}{K} L_p V \quad (5)$$

where ρ_L is the density of liquid alloy
g is the gravitational acceleration
h is the metallostatic head
R_p is the pouring rate (m/s)
H is the height of the molten metal at the lip of the pouring ladle
d_e is the equivalent capillary diameter
γ_{LV} is the liquid-vapor surface energy of the alloy
θ is the contact angle
μ is the dynamic viscosity of liquid metal
K is the permeability of the porous medium (sand)
L_p is the depth of penetration
V is the velocity of penetration.

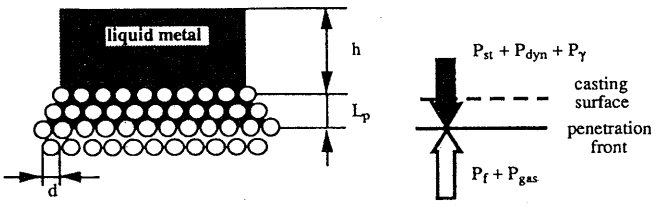

Fig. 1. Pressure balance during metal penetration in the molding aggregate.

In turn, the permeability of the porous medium is given by the Blake-Kozeny equation:

$$K = \frac{(1 - f_d)^3 d^2}{180 f_d^2} \quad (6)$$

where f_d is the fractional density and d is the average grain diameter. The penetration velocity can be calculated as:

$$V = \frac{L_P}{t_p} \quad (7)$$

where t_p is the solidification time of penetrating layer (penetration time), and, substituting Equations 2–7 in Equation 1, the penetration depth can be calculated as:

$$L_p = \left[\frac{d^2 t_p}{180 \mu} \frac{(1 - f_d)^3}{f_d^2} \left(\rho g h + 1.41 \rho R_p \sqrt{g(H - h)} + \frac{4}{d_e} \gamma_{LV} \cos\theta \right) \right]^{0.5} \quad (8)$$

It can be seen that L_p increases as the fractional density and the viscosity of the metal decrease, and as the sand grain diameter, the density of the melt and the solidification time increase. Whether penetration will occur at all or not, depends on the ratio between the static and dynamic pressure on one hand, and the capillary pressure on the other. Indeed,

if h = 0, and H = 0
- for θ = 90° $L_p = 0$ no penetration
- θ > 90° $P_\gamma < 0$ no penetration
- θ < 90° $L_p > 0$ **chemical penetration**

if h > 0 and H > 0
- for θ = 90° $L_p > 0$ **mechanical penetration**
- θ > 90° depending on the relative values of P_γ and P_{st} + P_{dyn}, penetration may occur or not
- θ < 90° **mechanical and chemical penetration**

It is interesting that the surface energy γ_{LV} may have opposing influences. Indeed, when θ > 90°, an increase in γ_{LV} will result in a decrease of L_p. The opposite is true for θ < 90°.

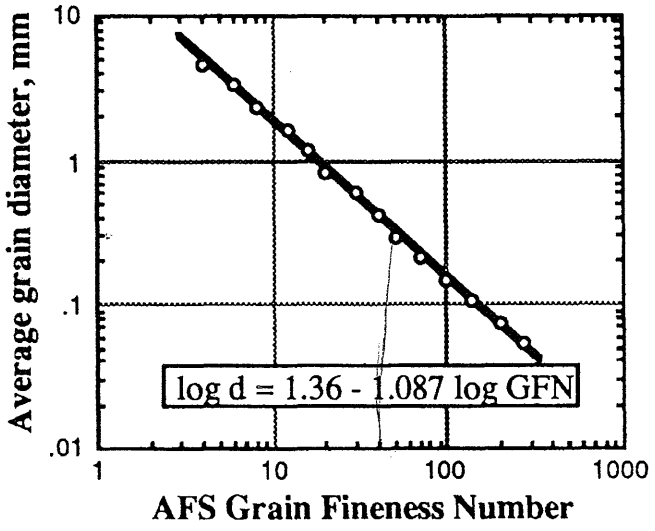

Fig. 2. Correlation between the average grain diameter and the grain fineness number.

EXPERIMENTAL

Evaluation of Parameters in the Penetration Equation

Grain Diameter

The average grain diameter can be directly related to the AFS grain fineness number (gfn) by using the screen scale sieves.[8] The correlation is shown in Fig. 2. The average grain diameter (mm) can be calculated directly from the gfn with the logarithmic relationship on the figure.

Fractional Density

The fractional density of a molding aggregate can be calculated as the ratio between the bulk density and the true density. It is also equivalent to the percent solids (f_d x 100). Since both the bulk density and the true density of molding materials can be measured, the fractional density can be obtained directly from experimental measurements. Typically, the fractional density of green molding sands varies between 39 and 70. The fractional density of dry molding sands varies between 54 and 64. Apparently, a direct relationship exists between fractional density and the hardness of compacted green sand, as shown in Fig. 3, based on data from Table 4.1 in Reference 9. However, it must be emphasized that, if data as those in Fig. 3 are to be used for evaluation of fractional density, considerably more data must be collected and evaluated.

Penetration Time

An accurate penetration time can only be obtained with numerical solidification models that describe the cooling of liquid metal as it penetrates the mold. In a first approximation, the penetration time, t_p, can be considered to be the time required for the liquid metal in the mold to loose all its superheat. Once the liquidus temperature is reached and solidification starts at the metal/mold interface, it can be assumed that penetration becomes impossible. Under this scenario, the penetration time can be calculated with the equation (see Appendix A for details):

$$t_p = \frac{\rho_L c_L \Delta T_{sup} M}{h(T_L - T_o + 0.5 \Delta T_{sup})} \quad (9)$$

where
- c_L is the specific heat of the liquid metal
- T_L is the liquidus temperature of the alloy
- T_o is the ambient temperature
- ΔT_{sup} is the superheat
- h is the metal/mold heat transfer coefficient
- M is the modulus of the casting.

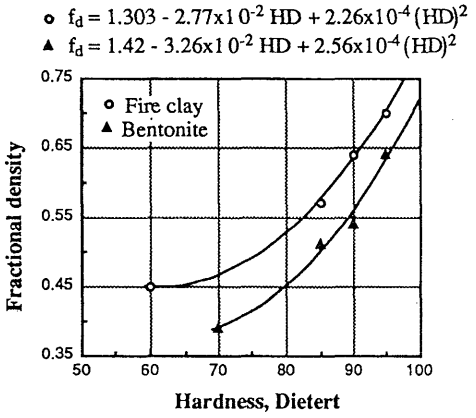

Fig. 3. Correlation between the fractional density and the Dietert hardness of green sand for tempered sands of 60–75 AFS gfn.

Equivalent Capillary Diameter

The equivalent capillary diameter, d_c, can be calculated or measured experimentally for different molding aggregates.

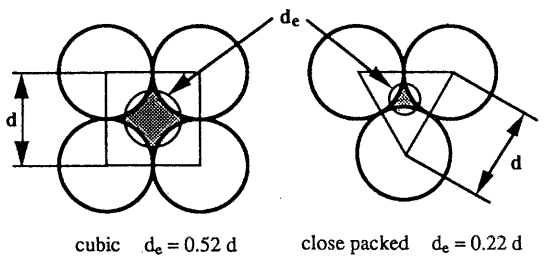

Fig. 4. Examples of calculation of equivalent capillary diameter.

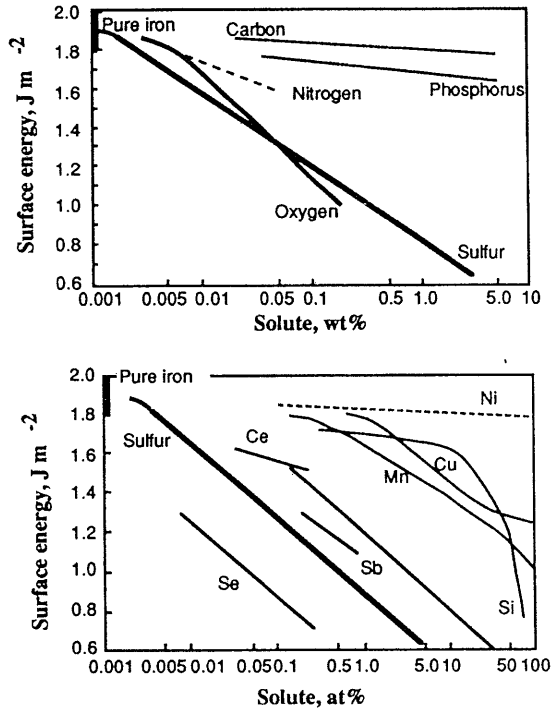

Fig. 5. Effect of various elements on the surface energy of liquid iron at 1550–1570C.[10]

Some simple examples of two-dimensional calculation of the equivalent capillary diameter are given in Fig. 4 for cubic and close-packed configurations. For the close-packed three-dimensional case, it can be shown that (see Appendix B for details):

$$d_e = 1.1\ d\ (1 - f_d)^{1/3} \qquad (10)$$

Thus, the capillary diameter is simply a function of average grain density, d, and of fractional density. It is also directly related to the permeability of the sand as measured by the AFS test.

Experimental evaluation of the equivalent capillary diameter can be done with a mercury porosimeter. Samples of the 5-mm molding aggregate were evacuated to 50 μm vacuum in the porosimeter's filling apparatus. The sample was then immersed in mercury and the pressure was gradually raised to atmospheric pressure while measuring the volume of mercury that had intruded into the pores of the sample. A direct calculation was used to evaluate the pore number distribution at each pore radius. From this curve, the average pore size was estimated. Some typical experimental data showing the correlation between the capillary diameter of dry sand samples, their hardness (before drying) and their permeability is shown in Table 1. It is apparent that, as the hardness of the sand increases, the permeability and the capillary diameter decrease.

Liquid-Vapor Surface Energy of Alloys

As shown in Fig. 5, increased contents of both nonmetals and metals decrease the surface energy of iron.[10] Oxygen, sulfur and nitrogen have a particularly strong influence. As pointed out earlier, when the metal is not wetting the mold ($\theta > 90°$) a decrease in γ_{LV} will result in increased penetration. Thus, an increase in the content of any elements will be conducive to higher penetration tendency, unless the contact angle is increased. As will be shown later, the contact angle also seems to decrease with the increase in the content of the vast majority of elements.

Contact Angle

The contact angle between the molten metal and the molding aggregate plays a major role in the occurrence of metal penetration. The major part of the experimental research effort has been devoted to the evaluation of the contact angle for various metal/molding aggregate couples. The experimental technique has been described in earlier publications.[7,11] Typically, metals do not wet the ceramic materials used as molding aggregates, but oxides and fayalite do, as shown in Fig. 6. A summary of our research findings on this issue, including some new data, is presented in the following paragraphs.

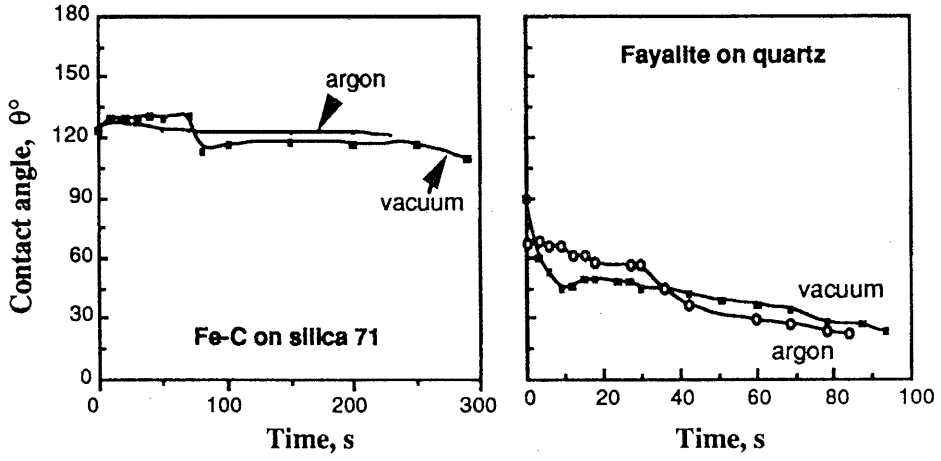

Fig. 6. Variation of contact angle of an iron-carbon alloy and of fayalite in time.[7]

Table 1.
Experimental Correlation Between the Green Hardness, Dry Permeability and Dry Capillary Diameter

Hardness	67	74	76.3	80
Permeability	425	424	350	333
Capillary dia., mm	0.11	0.10	0.11	0.094

Table 2.
Average Contact Angles for Individual Experiments

Experiment no.	1	2	3	4	5	6
Contact angle	125.3°	121.7°	122.5°	122.4°	122.1°	122.2°

Table 3.
Contact Angle Measurements for Various Molding Aggregates

Alloy	Carbon Equiv.	Chromite sand gfn 55	Silica sand gfn 108	Zircon sand gfn 106	Carbon sand
Fe-0.5C	0.5	106.1°	93.4°	125.8°	91.8°
Fe-3.7C	3.7	124.2°	95.8°		108.0°
Fe-3.7C-1.25Si	4.08		115.0°		

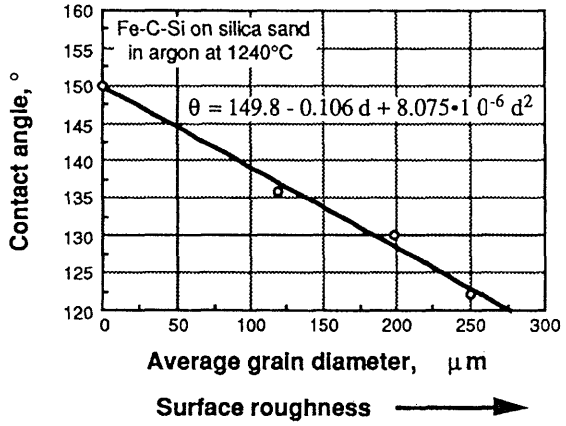

Fig. 7. Influence of grain size on contact angle.[11]

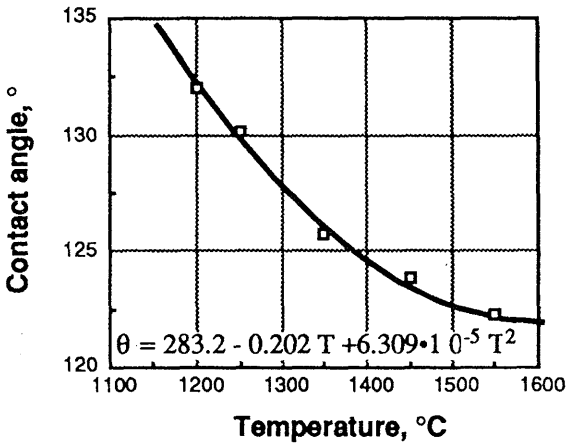

Fig. 8. Contact angle of synthetic Fe-C-Si alloy on silica sand (gfn 71) in argon atmosphere as a function of temperature.[11]

Evaluation of Contact Angle

Evaluation of Experimental Error

Six sessile drop experiments with a cast iron (3.43%C, 2.40%Si, 0.083%Mn, 0.13%P, 0.146%S) on monolithic quartz at 150C superheat were run. For each experiment, 18 contact angle measurements were performed at two-minute time intervals. The average contact angles over the time interval for the six experiments are given in Table 2. It was calculated that the mean contact angle was of 122.7° with a standard deviation of 1.1°.

Role of Surface Roughness of Ceramic Sample

The contact angle, as used in Equations 4 and 8, is an intrinsic material property. However, as shown in Fig. 7, the value of θ is a function of the surface roughness of the sample used in sessile drop experiments. In certain cases, it may not be possible to obtain monolithic samples for measurement. Nevertheless, by taking several measurements for samples made with grains of different sizes, it should be possible to extrapolate results to a monolithic substrate. Indeed, as shown in Fig. 7, the extrapolation of experimental results for various grain diameters hits the data point for monolithic quartz.

Influence of Temperature on Contact Angle

The temperature of the liquid metal in the mold will influence the value of the contact angle. As shown in Fig. 8, θ decreases as the temperature increases.

Contact Angles of Various Molding Materials

A number of experiments were conducted to assess the role of the type of molding aggregate on contact angle. The experimental results for measurements at 1600C are given in Table 3 and Fig. 9 as a function of the carbon equivalent of the alloy. It can be seen that the best behavior is exhibited by the zircon sand, which has the highest contact angle. It is also apparent that the contact angle increases as the carbon equivalent increases. These results should not be considered as definitive since limited previous work[11] with Fe-C-Si alloys seemed to indicate that the contact angle on zircon sand was smaller than on silica sand. As previously mentioned, grain fineness influences the value of the contact angle. These experiments should be repeated for monolithic substrates.

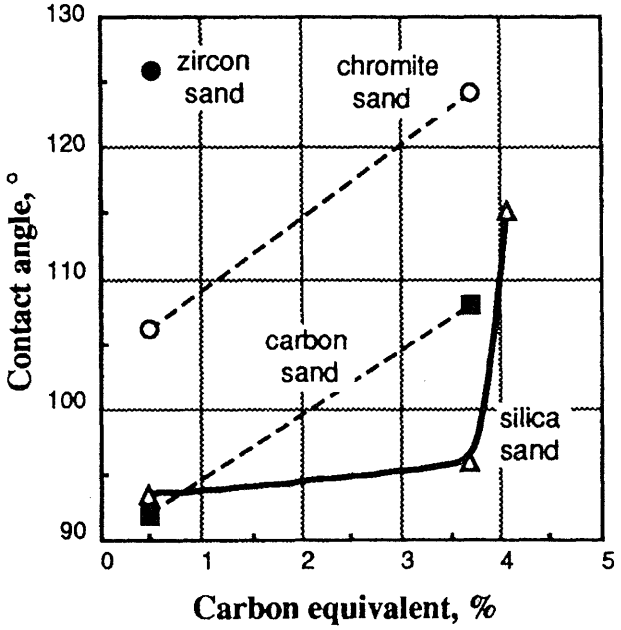

Fig. 9. Influence of the carbon equivalent of Fe-C alloys on their contact angles on various molding aggregates.

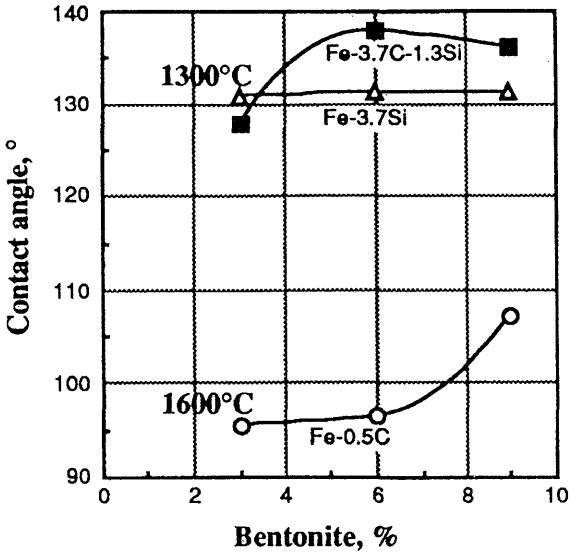

Fig. 10. influence of testing temperature and bentonite content of the silica sand on the contact angle of three types of Fe-C alloys.

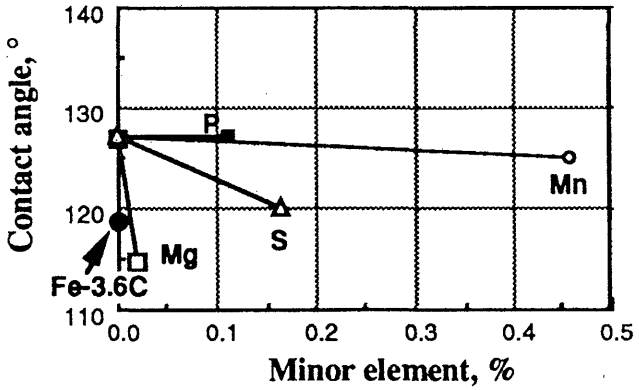

Fig. 11. Influence of minor elements on the contact angle at 1300C for commercial purity Fe-3.68C-1.25Si alloys on monolithic quartz substrate (for comparison, the data point of the Fe-3.6C alloy is also shown).[11]

Effect of Sand Additives on Contact Angle

The results of the influence of the bentonite content in silica sand on contact angle are given in Table 4 and Fig. 10. The data in Fig. 10 reflect the effects of both temperature and composition. Although the temperatures at which the measurements were performed were different, the superheating for all samples was 150C. Apparently, an increase in the bentonite content raises the contact angle. It is not clear, at this time, whether this increase is because of a lower metal/bentonite contact angle, or because bentonite decreases the roughness of the sample by filling the intergranular spaces. Again, the highest contact angle was recorded for the high carbon equivalent alloy.

Effect of Quaternary Elements on the Contact Angle of Fe-C-Si Alloys

From the data presented in Fig. 11, it is apparent that most elements decrease the contact angle. Silicon is a notable exception. In these experiments, as well as in the experiments presented in Fig. 9, a silicon addition to the Fe-C alloy substantially increased the contact angle. It is hypothesized that silicon decreases the oxygen content in the melt, which then results in a higher contact angle.

Effect of Mold Atmosphere on Contact Angle

The effect of the atmosphere on the contact angle is more difficult to assess through sessile drop experiments because of the complicated reactions that may occur in the apparatus. Nevertheless it is apparent that increasing the oxygen content or the CO_2/CO ratio results in a decrease of the contact angle. This is demonstrated through Fig. 12, which was derived from data previously presented.[11]

Table 4. Contact Angles Measured for Various Contents of Bentonite in Silica Sand gfn 71

Temperature Bentonite,%	1600°C Fe-0.5C	1300°C Fe-3.7C	1300°C Fe-3.7C-1.3Si
3	95.5	130.8	127.8
6	96.5	131.2	137.9
9	107.2	131.2	136

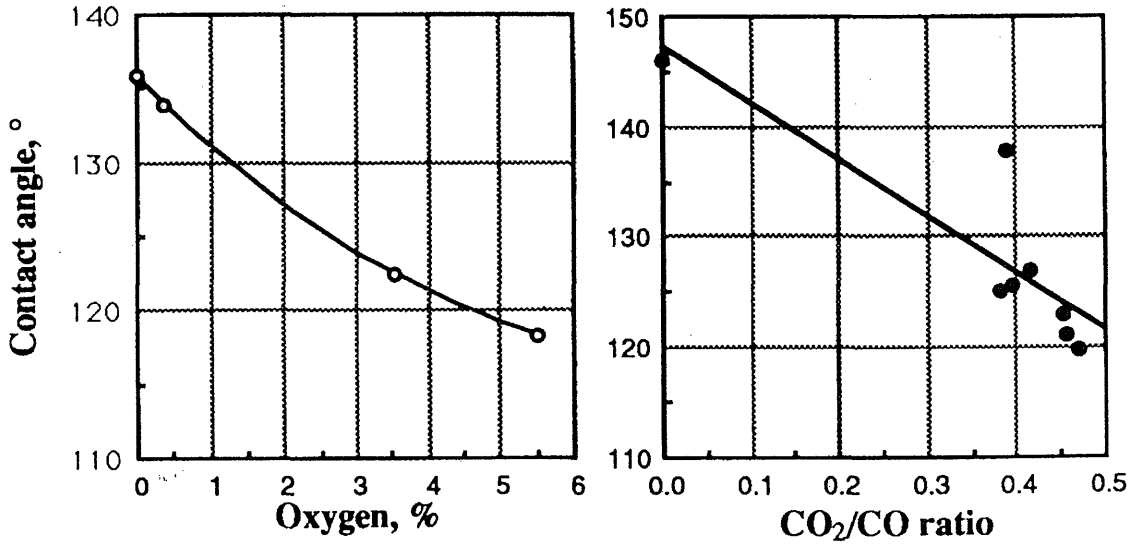

Fig. 12. Contact angle of synthetic Fe-C-Si alloy on silica sand 108 + 9% sodium bentonite in 95% argon + 5% oxygen atmosphere and in CO_2/CO atmosphere.

In a new set of experiments, an Fe-3.7C-1.25Si sample was melted at 1205C on a silica sand gfn 71 + 3% western bentonite substrate in the tube furnace. At the beginning of the experiment, the atmosphere was 100% argon. During the experiment, CO_2 was added to the argon stream, resulting in an increase in the CO_2 content in the furnace atmosphere. An attempt was made to stabilize the atmosphere composition at two different levels of CO_2: 7 and 14%. The experimental results, including the measured composition of the furnace atmosphere and the contact angles at different times, are given in Fig. 13. The data clearly indicate that the contact angle is continuously decreasing with increased CO_2 content in the atmosphere. Thus, it is demonstrated that an oxidizing atmosphere decreases the contact angle and, thus, favors penetration.

CALCULATION OF PENETRATION (MODEL VALIDATION)

Some preliminary calculations with the model were performed using the data in Table 5. In Fig. 14, it is shown that penetration depth decreases as the metal head, h, decreases, and as the fineness of the sand grain increases.

While the increase in the height of the casting significantly increases penetration, the solidification time alone does not seem to be important for determining the critical contact angle at which penetration starts (Fig. 15). This is in apparent contradiction to the floor knowledge that suggests that a large casting, which has a long solidification time, is more prone to penetration defects than a small

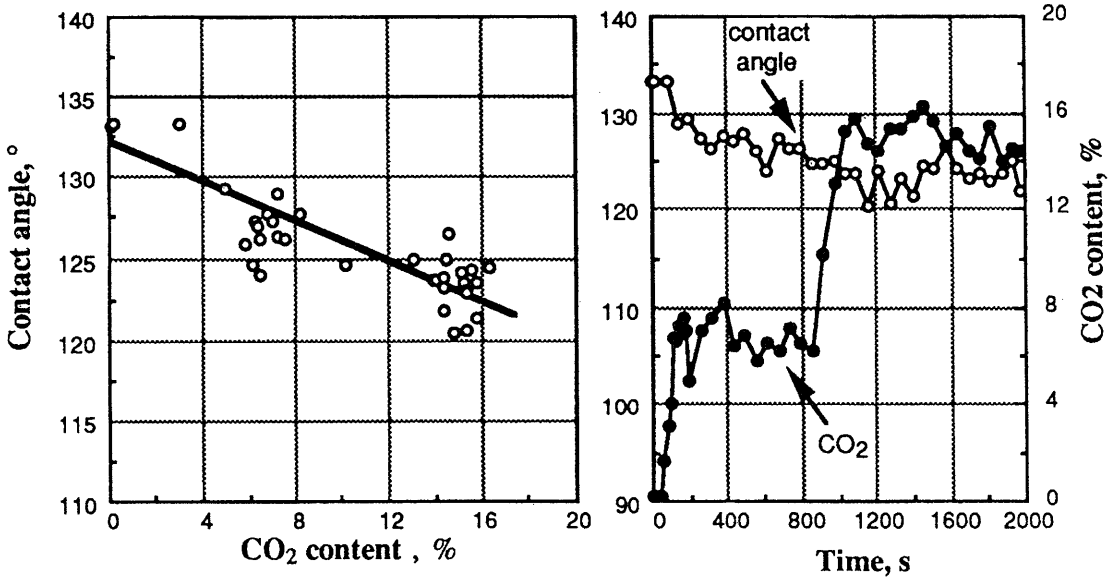

Fig. 13. Influence of increasing the CO_2 concentration in the furnace atmosphere over the contact angle.

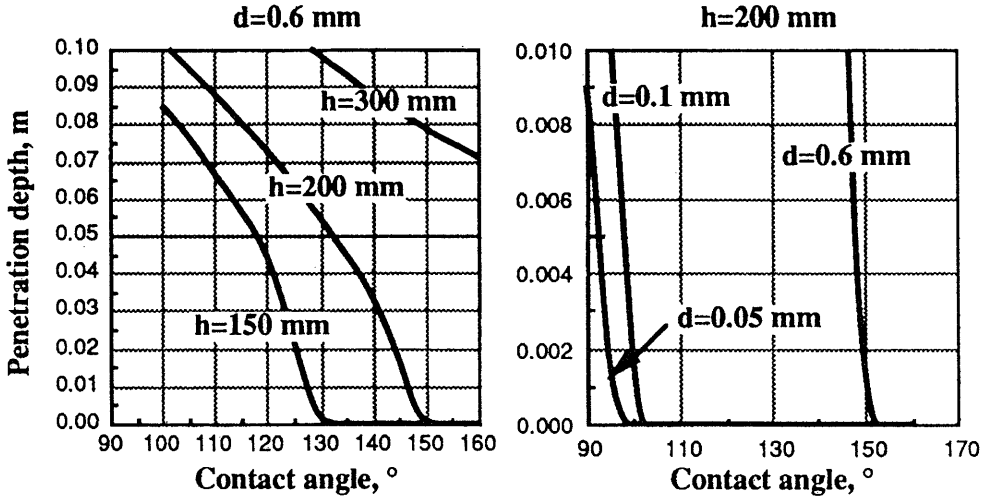

Fig. 14. Illustration of influence of contact angle on penetration length for iron castings molded in a sand packed at f_d = 0.65. Different casting heights and average grain sizes were assumed.

casting. It must be noted though that, typically, a larger casting will also have a higher metallostatic head, which will indeed result in larger penetration depth (see Fig. 14). Furthermore, the calculation in Fig. 15 assumes constant contact angle during penetration. While this assumption may be reasonable for small castings with short solidification times, it is increasingly invalid as the solidification time increases. Indeed, it is expected that, because of metal-atmosphere-mold reactions, the contact angle will decrease in time, resulting in larger penetration depth.

From Figs. 14 and 15, it is apparent that a critical contact angle for penetration exists for a given mold-metal-atmosphere system, above which penetration is not likely to occur, and under which penetration occurs very fast. It can be readily evaluated with Equation 8 if a penetration depth is defined. To illustrate the role of some mold variables on the critical angle for penetration, some calculations were performed assuming that L_p = 1 mm. The results are plotted in Fig. 16. As expected, the critical angle for penetration decreases (i.e., penetration is less probable) as the mold hardness or the fractional density increase.

Table 5. Typical Data Base for Calculation

Parameter	Units	Value	Comments
μ	Pa s	5.03×10^{-3}	for Fe at T_{melt}
g	m s^{-2}	9.81	
γ_{LV}	J m^{-2}	1.9	for Fe
ρ_m	kg m^{-3}	1500	for sand mold
ρ_L	kg m^{-3}	7000	for liquid cast iron
c_m	J kg^{-1} K^{-1}	360	for sand mold
c_L	J kg^{-1} K^{-1}	820	for liquid cast iron
h	W m^{-2} K^{-1}	3000	for metal/sand mold interface
T_L	K	1154	for cast iron
ΔT_{sup}	K	100	

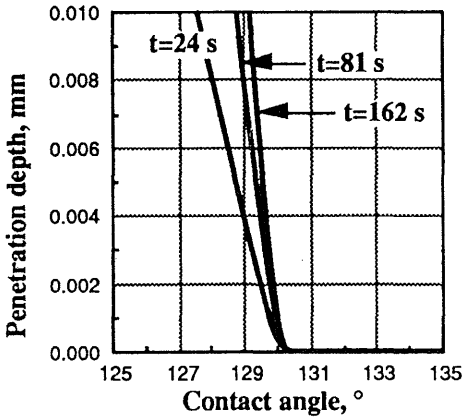

Fig. 15. Variation of penetration depth with contact angle and penetration time. Other data used in calculation are as follows: f_d = 0.65, h = 0.15 m, d = 0.6 mm. The penetration times of 24, 81 and 162 correspond to casting moduli of 0.15, 0.5 and 1, respectively.

CONCLUSIONS

A new model describing metal penetration into the molding aggregate has been introduced. The model was derived, based on the pressure balance at the metal/mold interface, and takes into account the following variables: average sand grain size (gfn), solidification time of the casting, fractional density of the mold (mold hardness), liquid metal viscosity and density, metallostatic pressure, pouring rate and contact angle between the metal and the molding aggregate. A description of the methods that can be used to evaluate these variables for different metal-mold couples was given. Illustrative examples of the use of the model to evaluate both the probability and the extent of penetration for various situations were also presented.

Sessile drop experimental work shows that higher carbon equivalent increases the contact angle and, thus, decreases the penetration tendency. Silicon addition seems to be particularly beneficial from this standpoint. All other elements tested (P, Mn, S, Mg) decrease the contact angle. Both chromite and zircon sand produce higher contact angles than silica sand. Bentonite additions to the silica sand also result in increased contact angle. It was also successfully demonstrated that an increase in the oxygen, CO_2, or CO_2/CO ratio in the atmosphere reduces the contact angle and, thus, is conducive to penetration.

ACKNOWLEDGMENTS

This work has been supported by AFS (grant no. 11-90-91) and by the U.S. Department of Energy (DOE Cooperative agreement No. DEFC07-92ID13163). However, any opinions, findings, conclusions or recommendations expressed herein are those of the authors and do not necessarily reflect the view of DOE.

The authors are pleased to acknowledge the active support of the monitoring committee and, in particular, the direct involvement of L. Stahl, W. Marchisin, D. Jablonski and P. Carey. Mr. Dan Twarog has also gracefully contributed his knowledge and time to both the technical and financial aspects of this project. The authors are also indebted to Spectro Analytical Instruments for the generous donation of a Spectrolab on which the chemical analyses of the alloys were run.

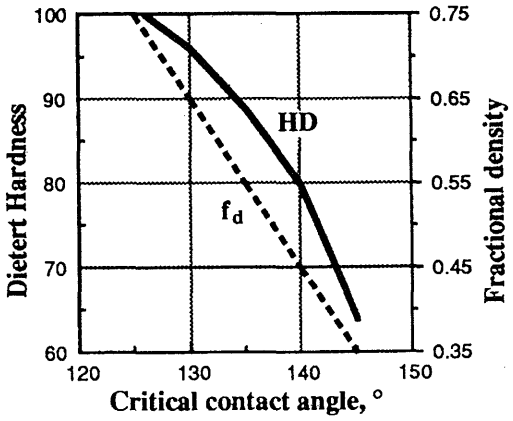

Fig. 16. Variation of critical contact angle with fractional density or mold hardness. Other data used in the calculation are: h = 0.15 m, d = 0.6 mm, t_p = 24 sec.

APPENDIX A

Calculation of the Penetration Time

It is assumed that the metal can penetrate into the molding aggregate only until solidification begins at the metal/mold interface. it is further assumed that solidification at the metal/mold interface starts as soon as the liquid metal has lost all its superheating.

Assuming that the average interface temperature on the metal side is $T_L + 0.5\,\Delta T_{sup}$, the heat flux going into the mold can be calculated as:

$$q = -h\left(T_L + \frac{\Delta T_{sup}}{2} - T_o\right) \tag{A1}$$

where h is the metal/mold heat transfer coefficient
T_L is the liquidus temperature of the alloy
ΔT_{sup} is the superheating
T_o is the ambient temperature.

The heat flux out of the metal is:

$$q = -\rho_L c_L \Delta T_{sup} \frac{dx}{dt} \tag{A2}$$

where ρ_L, c_L are the density and specific heat of the liquid metal, respectively. Equating Equations A1 and A2 and integrating one obtains:

$$t_p = \frac{\rho_L c_L \Delta T_{sup} M}{h\left(T_L - T_o + 0.5\,\Delta T_{sup}\right)} \tag{A3}$$

where t_p is the penetration time, and M = V/A is the modulus of the casting.

APPENDIX B

Calculation of Equivalent Capillary Diameter

Assume that the sand grains are spherical in shape, have the same size and are packed as in a face-centered cubic lattice (Fig. B1). Not all the sites must be filled by sand grains. The number of unfilled sites depends on the fractional density.

The total volume of grains in a cubic volume element of packed sand is:

$$V_{gr} = n\left(\frac{4}{3}\pi r^3\right) \tag{B1}$$

where n is the number of positions per cubic volume element that can be occupied by grains, and r is their average radius. The volume of the cubic elemental volume is:

$$V_c = 4\,(n - m)\sqrt{2}\,r^3 \tag{B2}$$

where m is the number of missing grains per volume element. The fractional density within the volume element is:

$$f_d = \frac{V_{gr}}{V_c} = \frac{n\left(\frac{4}{3}\pi r^3\right)}{4\,(n - m)\sqrt{2}\,r^3} \tag{B3}$$

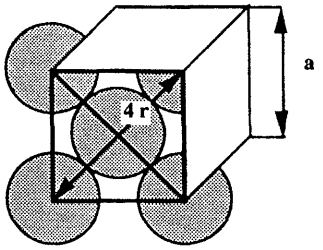

Fig. B1. Hypothetical packing of sand grains in the mold.

Thus, the number of grains per volume element is calculated to be:

$$n - m = \frac{\pi}{3\sqrt{2}}\frac{n}{f_d} \tag{B4}$$

The volume of voids associated with one grain is:

$$V_v = \frac{V_c - V_{gr}}{n - m} = 4\sqrt{2}\,r^3\,(1 - f_d) = \frac{4}{3}\pi r_e^3 \tag{B5}$$

where r_e is the equivalent capillary radius. Finally, the capillary diameter is:

$$d_e = 1.1\,d\,(1 - f_d)^{1/3} \tag{B6}$$

Note that this derivation assumes that all sand grains are of the same size. The use of a three-screen or four-screen sand will give an equivalent capillary diameter smaller than the value calculated with Equation B6.

REFERENCES

1. G.A. Colligan, L.H. Van Vlack and R.A. Flinn, "The Effect of Temperature and Atmosphere on Iron-Silica Interface Reaction," *AFS Transactions,* vol 66, 1958, p 457.
2. A.B. Draper and J.L. Gaindhar, "Metal Penetration—A Critical Literature Review," AFS Research Report, 1977, p 164.
3. J.M. Svoboda and G.H. Geiger, "Mechanism of Metal Penetration in Foundry Molds," *AFS Transactions,* vol 77, 1969, pp 281.
4. W.D .Scott, P.A. Goodman and R.W. Monroe, "Gas Generation at the Mold-Metal Interface," *AFS Transactions,* vol 86, 1978, pp 599-610.
5. R.A. Flinn, L.H. Van Vlack and G.A. Colligan, "Mold-Metal Reactions in Ferrous and Nonferrous Alloys," *AFS Transactions,* vol 94, 1986, pp 29-46.
6. P. Delannoy, D.M. Stefanescu and T.S. Piwonka, "A Critical Literature Review of Theories for the Formation of Casting Metal Penetration Defects," AFS Research Report #2, April, 1990, pp 4-26.
7. D.M. Stefanescu, P. Delannoy, T.S. Piwonka and S. Kacar, "An Investigation in the Role of Sand-Metal Contact Angle in the Formation of Casting Penetration Defects," *AFS Transactions,* vol 99, 1991, pp 761-780.
8. "Particle Size Distribution of Foundry Sand Mixtures," *Mold and Core Test Handbook,* American Foundrymen's Society, 1978, p 4-1 to 4-14.
9. R.W. Heine, C.R. Loper, Jr. and P.C. Rosenthal, *Principles of Metal Casting,* Mc-Graw-Hill Book Co., New York, 1967.
10. B.C. Allen, "The Surface Tension of Liquid Metals," *Liquid Metals: Chemistry and Physics,* S.Z. Beer, editor, Marcel Dekker Inc., New York, 1972.
11. S. Giese, D.M. Stefanescu, T.S. Piwonka, S. Sen and B.K. Dhindaw, "An Investigation on the Role of Sand-Metal Contact Angle in the Formation of Casting Penetration Defects: Phase II" *AFS Transactions,* vol 100, 1992, p 785.